FEATURE ARTICLE

Electronic Quenching of OH A $^2\Sigma^+$ ($v' = 0, 1$) in Complexes with Hydrogen and Nitrogen

Marsha I. Lester,* Richard A. Loomis,† and Rebecca L. Schwartz†

Department of Chemistry, University of Pennsylvania, Philadelphia, Pennsylvania 19104-6323

Stephen P. Walch

NASA Ames Research Center, Thermosciences Institute, MS-230-3, Moffett Field, California 94035-1000

Received: August 22, 1997[⊗]

The quenching of electronically excited OH A $^2\Sigma^+$ radicals has been investigated in complexes of OH with molecular hydrogen, deuterium, and nitrogen and through complementary theoretical calculations. Many of the intermolecular vibrational levels supported by the OH A $^2\Sigma^+$ ($v' = 0, 1$) + H_2, D_2, and N_2 potentials have been characterized by laser-induced fluorescence and fluorescence depletion measurements of the complexes in the OH A $^2\Sigma^+$−X $^2\Pi$ 1−0 and 0−0 spectral regions. Homogeneous line broadening of the spectral features yields picosecond lifetimes for complexes prepared in levels derived from OH A $^2\Sigma^+$ ($v' = 0$) as a result of electronic quenching and/or chemical reaction. More extensive line broadening is observed for complexes excited to levels correlating with OH A $^2\Sigma^+$ ($v' = 1$). The corresponding decay rates are 10−75 times faster than obtained for $v' = 0$ due to the opening of the vibrational predissociation channel and/or enhancement of the quenching/reaction processes upon OH vibrational excitation. Ab initio calculations of the OH (A $^2\Sigma^+$, X $^2\Pi$) + H_2 and N_2 potential energy surfaces reveal the minimum energy configurations, T-shaped O−H--H_2 and linear O−H--N≡N, and the large increases in interaction energy upon electronic excitation of OH. The theoretical calculations also identify specific orientations, T-shaped H−O--H_2 and linear H−O--N≡N, that lead to conical intersections between the ground- and excited-state surfaces and give rise to quenching of OH A $^2\Sigma^+$ by hydrogen and nitrogen.

I. Introduction

The hydroxyl radical plays a pivotal role in atmospheric[1,2] and combustion[3,4] chemistry. As a result, the concentration, temperature, and lifetime of the OH intermediate are sensitive probes of the complex chemistry taking place in these environments. The OH radicals are often monitored in these surroundings by the laser-induced fluorescence (LIF) method on the A $^2\Sigma^+$−X $^2\Pi$ electronic transition.[5] Collisions with molecular partners prevalent in these situations, however, are known to quench the OH A $^2\Sigma^+$ fluorescence in a quantum state specific manner,[6] thereby preventing quantitative measurements of the OH ground-state population distribution (number density, temperature, etc.) by LIF. Methods have been developed to try to circumvent this problem, for example, by exciting OH to a rapidly predissociating level in the excited A $^2\Sigma^+$ electronic state[7,8] or through direct absorption measurements. Others have systematically measured the state specific rate constants for electronic quenching of OH A $^2\Sigma^+$ by the predominant gases and at the relevant temperatures present in these environments.[6] This provides the database needed to correct for collisional quenching effects in OH LIF measurements in these complex kinetic systems.

This feature article focuses on the quenching of electronically excited OH A $^2\Sigma^+$ radicals by simple molecular partners, specifically hydrogen and nitrogen, which are of both fundamental and practical importance. We seek to answer the following questions: What are the characteristics of the OH A $^2\Sigma^+$ + H_2 and N_2 intermolecular potential energy surfaces? Are there deep potential wells on these surfaces that might play a role in the electronic quenching of OH A $^2\Sigma^+$ by H_2 or N_2? Are there specific orientations of the partners that preferentially lead to quenching? What is the mechanism for quenching of OH A $^2\Sigma^+$ by these partners and what products are formed?

These questions are addressed through spectroscopic and dynamical studies of electronically excited OH A $^2\Sigma^+$ ($v' = 0$, 1) in complexes with molecular hydrogen, deuterium, and nitrogen.[9−12] In addition, complementary ab initio calculations have been carried out to characterize the OH (A $^2\Sigma^+$, X $^2\Pi$) + M, where M = H_2, D_2, and N_2, potential energy surfaces.[13−18] The theoretical calculations reveal—for the first time—the origins of electronic quenching in these systems by identifying the locations of conical intersections[19] that funnel molecules from the OH A $^2\Sigma^+$ + M potential energy surface to either the OH X $^2\Pi$ + M surface or to reaction products.[17,18] The experimental results are then interpreted in light of these theoretical calculations. We begin with a brief survey of previous work on these systems.

A. Collisional Studies of Quenching and Vibrational Energy Transfer. Collisional deactivation (quenching) of electronically excited OH A $^2\Sigma^+$ radicals by ground-state partners has received much attention over the years. Several experimental studies have been performed to determine the rate constants and cross sections for collisional quenching of OH A $^2\Sigma^+$ by H_2, D_2, N_2, and other partners.[20−26] Here, quenching

† Present address: JILA, National Institute of Standards and Technology and University of Colorado, and Department of Chemistry and Biochemistry, University of Colorado, Boulder, CO 80309-0440.

⊗ Abstract published in *Advance ACS Abstracts,* November 15, 1997.

S1089-5639(97)02755-2 CCC: $14.00

TABLE 1: Quenching (Q0 and Q1) and Vibrational Energy Transfer (VET) Cross Sections (σ) for OH A $^2\Sigma^+$ ($v' = 0, 1$) in Its Lowest Rotational Levels with Various Collision Partners at Room Temperature

collision partner	σ_{Q0} (Å^2)	σ_{Q1} (Å^2)	σ_{VET} (Å^2)	ref
H_2	7.4	7.7	9.7	20
	4.6		9.7	21
	9.3			22
	11.6			23
D_2	7.4		15.9	21
	11.0			23
N_2	3.4	3.9	19.6	20
	5.8		24.7	21
	5.3			22
	6.7			23
	7			24
			36	32
	5.3	8	32	25
	3.6	0.4	30	26[a]
Ar	0.4			21
			0.6	26[a]

[a] Values are for a thermal distribution at 300 K.

is defined as the collision-induced removal of OH population (decrease in spontaneous emission) from an initially prepared OH A $^2\Sigma^+$ (v', n') rovibrational level via nonradiative decay channels. Early studies indicated that hydrogen quenches OH A $^2\Sigma^+$ in $v' = 0$ and $v' = 1$ with nearly identical cross sections of 7.4 and 7.7 Å^2, respectively.[20] More recently, quenching cross sections of 11.6 and 11.0 Å^2 were measured for collisions of H_2 and D_2 with OH A $^2\Sigma^+$ ($v' = 0$).[23] Nitrogen was found to be less efficient than H_2/D_2 in quenching OH A $^2\Sigma^+$ prepared in levels both with and without vibrational excitation. The quenching cross sections for OH A $^2\Sigma^+$ prepared in specific rovibrational levels with these molecular partners are summarized in Table 1; the negligible value for quenching by argon is listed for comparison.

For each of these molecular collision partners, the rate of quenching was strongly dependent on the initial OH A $^2\Sigma^+$ rotor level n', decreasing with increasing rotational excitation.[23] This rotational level dependence has led to the hypothesis that quenching occurs as a result of collision complexes that are formed because of anisotropic, long-range attractive forces between the excited OH and its collision partner; increasing rotation of the OH causes the orientational dependence of the approach of the two partners to be averaged out.[6] This view is also consistent with temperature-dependent studies of quenching in OH, where an increase in the collision energy (temperature) results in a decrease in quenching.[27−30] Finally, Paul has proposed a model for the temperature-dependent collisional quenching of OH A $^2\Sigma^+$ based on a harpoon mechanism;[31] the underlying concept of a "crossing" between two potential energy surfaces, though not involving electron transfer, is borne out in the ab initio calculations presented in section VII.

The rate constants and cross sections (Table 1) for downward vibrational energy transfer (VET) in the A $^2\Sigma^+$ state of OH have also been examined for these same collision partners.[20,21,25,26,32,33] For H_2 and D_2, the VET cross sections are comparable to their respective quenching values and follow a similar rotational level dependence.[21] Vibrational relaxation of OH A $^2\Sigma^+$ ($v' = 1$) by N_2 is found to be far more efficient than quenching. For N_2, the cross section for VET was determined to be on the order of gas kinetic and decreased sharply with increasing rotational level. Again, this suggests that anisotropic, attractive forces lead to the formation of a transitory collision complex that plays a role in the VET process.

B. Dynamical Processes in OH−H$_2$, −D$_2$, and −N$_2$ Complexes. In full collisions, the quenching and vibrational relaxation processes were investigated under conditions that average over all orientations and impact parameters of the collision pair as well as sample a thermal distribution of velocities at 298 K. Recently, the analogous dynamical processes have been examined following excitation of OH−M complexes to the OH A $^2\Sigma^+$ electronic state with zero or one quantum of OH vibrational excitation.[9−12] Here, the partners are brought together under the restricted geometry conditions of the OH−M ground-state complex and are then prepared in the excited OH A $^2\Sigma^+$ electronic state with well-defined intermolecular excitation. Homogeneous line broadening of the OH−M spectra in the OH A−X 1−0 and 0−0 regions (see section VI) reveals that dynamical processes are occurring on a picosecond or sub-picosecond time scale in OH−M complexes.

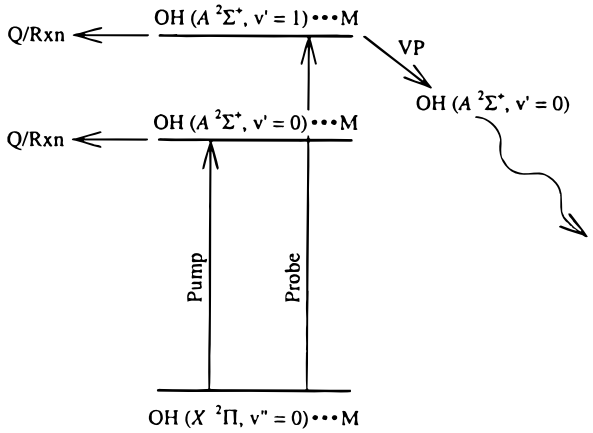

Figure 1. Schematic diagram of the principal decay channels that may occur upon electronic excitation of the OH−M complexes, where M = H_2, D_2, or N_2. Complexes promoted to the OH A $^2\Sigma^+$ electronic state with zero quanta of stretch ($v' = 0$) undergo rapid electronic quenching, Q, or reaction, Rxn, precluding their detection via laser-induced fluorescence. Complexes prepared with one quantum of OH vibrational excitation in the A state may decay via vibrational predissociation, VP, giving rise to emission from OH A $^2\Sigma^+$ ($v' = 0$) fragments, as well as through nonradiative Q/Rxn processes. Also shown are the pump and probe transitions used for fluorescence depletion experiments. Each time the pump laser is resonant with an OH−M transition, the ground-state population is reduced, resulting in a decrease in the probe laser-induced fluorescence signal.

The principal decay channels available when OH−M complexes are prepared in the excited OH A $^2\Sigma^+$ electronic state with zero or one quantum of OH stretching excitation are depicted in Figure 1. For OH−M complexes with OH A $^2\Sigma^+$ ($v' = 1$), these channels include electronic quenching and/or reaction (Q/Rxn), vibrational predissociation (VP), and radiative decay of the complex itself. The pathways of electronic quenching and chemical reaction are both referred to as "quenching" in the collision studies. Vibrational predissociation, the analog of VET in complexes, produces OH A $^2\Sigma^+$ ($v' = 0$) fragments which subsequently fluoresce on the A−X 0−0 transition; the electronic quenching and/or reaction channels are nonradiative decay pathways. For OH−M complexes prepared in levels derived from OH A $^2\Sigma^+$ ($v' = 0$) + M, the vibrational predissociation decay channel is closed. The nonradiative pathways of electronic quenching and chemical reaction are, therefore, the only avenues competing with radiative decay of the excited-state complex. These nonradiative decay processes are significant for OH−H_2, −D_2, −N_2 and other molecular partners, but are of negligible importance in systems such as OH−Ar.[34]

The remaining parts of this paper are organized as follows: Section II describes the OH (A $^2\Sigma^+$, X $^2\Pi$) + H_2 and N_2 potential energy surfaces derived from ab initio calculations.

Section III presents the experimental methods used to generate and characterize OH−H_2, −D_2, and −N_2 complexes. Section IV summarizes the spectroscopic findings, which are then used in section V to estimate binding energies for OH (A $^2\Sigma^+$, X $^2\Pi$) with H_2, D_2, and N_2. Section VI reveals the picosecond and sub-picosecond excited-state lifetimes for OH−H_2, OH−D_2, and OH−N_2 complexes which are derived from the homogeneous line broadening of experimental spectra. Finally, section VII discusses the origins of electronic quenching in the OH A $^2\Sigma^+$ + H_2 and N_2 systems.

II. Theoretical Background

A. Ab Initio OH (X $^2\Pi$, A $^2\Sigma^+$) + H_2 Potentials. The entrance channel for the OH X $^2\Pi$ + H_2 → H_2O + H reaction has been mapped out theoretically in a 1981 ab initio calculation by Kochanski and Flower[13] as well as in more recent computations by Clary, Werner, and co-workers[16] (MCKW) and by Offer and vanHemert;[15] these calculations do not consider the reactive regions of the potential. As the OH and H_2 reactants approach one another, they experience attractive multipole interactions, dominated by dipole−quadrupole and quadrupole−quadrupole forces, which lead to the formation of a shallow well in the entrance channel to reaction. The minimum of the average ground-state potential occurs in a symmetric T-shaped configuration with the H of the OH monomer pointing toward the H_2 monomer and has a depth of 188 cm^{-1} at an intermolecular separation distance of 3.2 Å.[16] Figure 2 illustrates a radial cut of the intermolecular potential in the minimum energy T-shaped structure. Here, *R* is defined as the distance between the OH and H_2 centers-of-mass. The barriers to internal rotation of the H_2 and OH monomers are predicted to be 470 and 210 cm^{-1}, respectively, though the barrier to the "geared bending" motion in which the OH and H_2 subunits move in a concerted fashion is significantly lower in energy.[16] Calculations of the bound states for *para*- and *ortho*-H_2 with OH, the far and near-infrared spectra of OH−H_2, and integral cross sections for rotationally inelastic scattering have been carried out based on these ab initio potentials.[14,16,35,36] The bound states and spectra of OH−H_2 complexes are found to be highly sensitive to the topology of the OH X $^2\Pi$ + H_2 potential in the entrance valley.

Ab initio calculations of the excited-state potential correlating with OH A $^2\Sigma^+$ + H_2/D_2 have revealed an ∼2000 cm^{-1} deep attractive well at the intermolecular bond length of ∼2.1 Å in a T-shaped O−H--H_2 configuration, as shown on a radial cut of the OH A $^2\Sigma^+$ + H_2 potential in Figure 2.[16,17,37] This is the same minimum energy geometry as found for the ground state; however, the calculations predict that the well depth will increase 10-fold and the intermolecular bond length will decrease by ∼1 Å upon A $^2\Sigma^+$ ←X $^2\Pi$ excitation of the OH moiety. These dramatic changes in the intermolecular potential upon electronic excitation permit many of the excited intermolecular levels supported by the OH A $^2\Sigma^+$ + H_2/D_2 potential to be accessed by electronic spectroscopy of OH−H_2/D_2 complexes.[38] OH A $^2\Sigma^+$ may also undergo chemical reaction or quenching with H_2 in a T-shaped H−O--H_2 configuration (180° internal rotation of OH from the minimum energy configuration). Ab initio calculations have identified a pathway that starts from the excited electronic state in this configuration and leads down to a conical intersection, producing H_2O + H (reaction) or OH X $^2\Pi$ + H_2 (quenching).[17] This aspect of the ab initio calculations will be considered in detail in section VII.B.

B. Ab Initio OH (X $^2\Pi$, A $^2\Sigma^+$) + N_2 Potentials. The intermolecular potential computed for OH X $^2\Pi$ with N_2 exhibits a minimum in a linear O−H--N≡N configuration,[18] with the interaction dominated by dipole−quadrupole forces. The well depth is 460 cm^{-1} at an intermolecular separation distance of 3.9 Å. Ab initio calculations of the interaction between electronically excited OH A $^2\Sigma^+$ and N_2 reveal a deep well in the linear O−H--N≡N configuration,[18] the same minimum energy configuration found for the ground electronic state. The excited-state potential has a well depth of 3770 cm^{-1} at an intermolecular separation of 3.0 Å. Radial cuts of the ab initio potentials in the linear O−H--N≡N configuration are shown in Figure 3. A substantial increase in the well depth and decrease in the intermolecular bond length occurs upon OH A←X electronic excitation. This provides Franck−Condon access to many of the intermolecular levels supported by the OH A $^2\Sigma^+$ + N_2 potential from ground-state OH−N_2 complexes. Electronically excited OH A $^2\Sigma^+$ may also be quenched by N_2 in the H-O--N≡N configuration; ab initio calculations[18] have mapped out the pathways that couple the ground and excited electronic states as discussed in section VII.C.

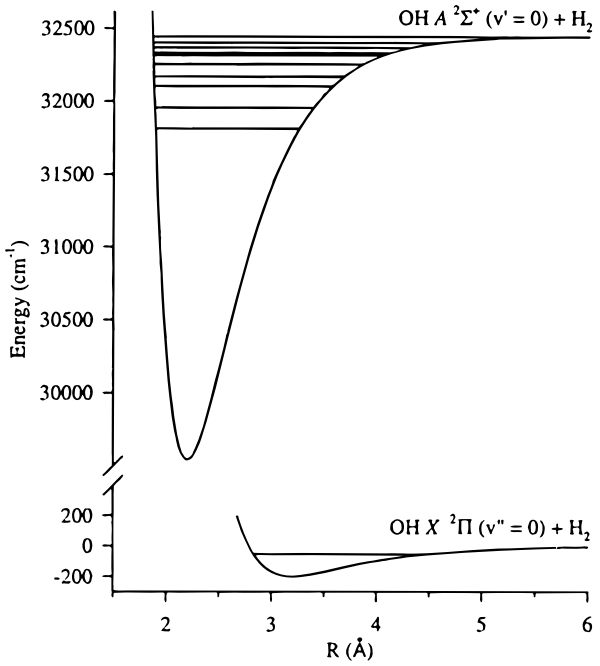

Figure 2. Radial cuts (*R*) through the ground, OH X $^2\Pi$ + H_2, and electronically excited, OH A $^2\Sigma^+$ + H_2, ab initio potential energy surfaces in the T-shaped OH−H_2 minimum energy configuration. The intermolecular vibrational levels observed in fluorescence depletion experiments are shown within the potentials. Ab initio potentials from refs 16 and 17.

III. Experimental Techniques

A. Stabilization of Complexes Correlating with OH X $^2\Pi$ + $H_2/D_2/N_2$. The experimental method used to produce OH−M complexes has been described previously.[10−12,39] Briefly, OH radicals are created by photolyzing gaseous nitric acid entrained in a carrier gas mixture using the 193 nm output of an ArF excimer laser. A 30% H_2 (or D_2), balance He, mixture is used as the carrier gas for the hydrogen (or deuterium) studies, while a 10% N_2 in He mixture is used for the nitrogen studies. The gas mixture is pulsed into the vacuum apparatus through a solenoid valve which incorporates a Peltier cooling element to reduce the temperature of the carrier gas and nitric acid. Photolysis occurs within a quartz capillary tube which is affixed to the pulsed valve assembly to facilitate precooling of the hydroxyl radical and diatomic partner prior to supersonic expansion. Weakly bound complexes of OH X $^2\Pi$ with H_2, D_2, or N_2 are then formed as the gas mixture undergoes supersonic expansion into the vacuum chamber. The precooling

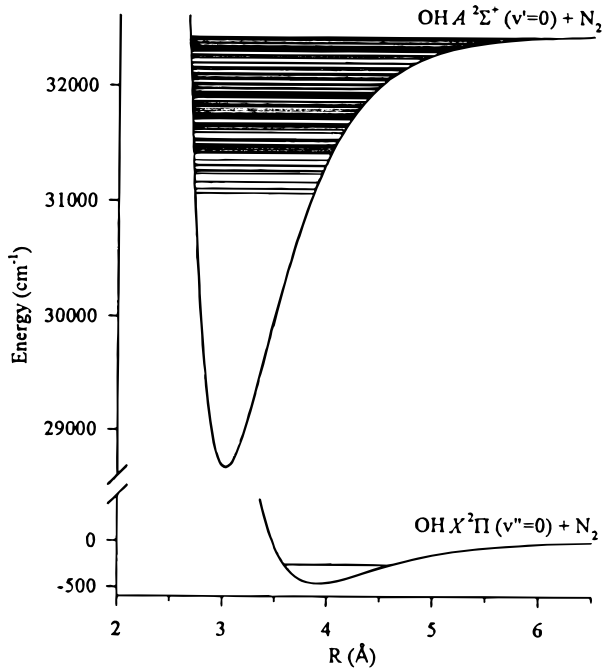

Figure 3. Radial cuts (R) of the ab initio potentials for OH (X $^2\Pi$, A $^2\Sigma^+$) + N_2 in the linear O−H--N≡N minimum energy configuration. Also shown are the intermolecular vibrational levels of OH−N_2 detected through fluorescence depletion measurements. Ab initio potentials from ref 18.

of the OH monomer has the added advantage of reducing the number and intensity of overlapping OH rotational lines lying within the spectral regions investigated.

The production of OH−H_2/D_2 entrance channel complexes requires a fine balance of the experimental parameters (photolysis position, carrier gas pressure, and pulsed valve temperature). OH−H_2 complexes are predicted to be bound by only 42 cm^{-1},[16] and thus extensive collisional cooling is required. These same collisions may also result in reaction, particularly in the early stages of the supersonic expansion, when the photolytically generated OH radicals have sufficient kinetic energy[40] to react with H_2/D_2 by surmounting or tunneling through the activation barrier to reaction (2100 cm^{-1}).[41,42] With increasing distance downstream in the expansion, the reaction rate decreases as the temperature and collision frequency drop until the reactants become cold enough to be stabilized within the shallow potential well in the entrance channel to the OH X $^2\Pi$ + H_2 reaction. The formation of the OH−H_2/D_2 prereactive complexes was optimized by using backing pressures as high as 200 psi (30% H_2/D_2 in He) and by cooling the pulsed valve assembly to −20 °C.

In contrast, the OH−N_2 complexes are significantly more well bound, ∼250 cm^{-1},[12] and the OH X $^2\Pi$ + N_2 partners are not reactive in their ground states. As a result, less extreme expansion conditions were necessary for optimum production of OH−N_2 complexes. Backing pressures of 150 psi (10% N_2/He) were used, and cooling of the pulsed valve did not further enhance complex formation.

B. Laser-Induced Fluorescence Experiments. The OH−M complexes have been characterized via electronic spectroscopy in the OH A $^2\Sigma^+$−X $^2\Pi$ region by both laser-induced fluorescence (LIF) and fluorescence depletion (FD) methods.[9−12] In the LIF experiments, the frequency-doubled output of a single Nd:YAG-pumped dye laser was used to excite ground-state OH−M complexes to intermolecular vibrational levels associated with either OH A $^2\Sigma^+$ ($v' = 0$) + M or OH A $^2\Sigma^+$ ($v' = 1$) + M. The laser beam was gently focused and intersected the supersonic gas expansion 1.5 cm downstream from the exit of the quartz capillary. The resultant fluorescence was collected with a telescope assembly and imaged onto a blue-sensitive photomultiplier tube positioned perpendicular to both the molecular and laser beam axes. In most experiments, a narrow bandpass filter, centered at 310 nm with a bandwidth of 20 nm, was used to limit the fluorescence collected to the OH A−X 1−1 or 0−0 spectral windows. In some experiments, the emission was dispersed with a 0.25 m monochromator (60 cm^{-1} resolution) which was positioned between the collection optics and the photomultiplier tube.

C. Fluorescence Depletion Experiments. Fluorescence depletion (FD) experiments were performed to probe the OH−M intermolecular vibrational levels correlating with OH A $^2\Sigma^+$ ($v' = 0$) + M which could not be detected by LIF due to rapid electronic quenching.[11,12] In these experiments, the frequency-doubled outputs of two tunable dye lasers, designated as the pump and probe lasers, were counterpropagated through the vacuum apparatus 1.5 cm downstream from the exit of the quartz capillary. The pump laser was operated in the 608−639 nm range and after frequency-doubling accessed the OH A−X 0−0 spectral region, while the probe laser worked in the 559−585 nm range accessing the OH A−X 1−0 region after doubling. The probe laser was optically delayed by 12 ns with respect to the pump laser. The fluorescence induced by the pump and/or probe lasers was collected in the same manner as described above for the LIF experiments.

A schematic diagram of the FD experiment is shown in Figure 1. The wavelength of the *pump* laser was *scanned* through the OH A−X 0−0 region, promoting OH−M from its lowest intermolecular level in the ground electronic state to various intermolecular vibrational levels supported by the OH A $^2\Sigma^+$ ($v' = 0$) + M potential. Each time the pump laser was resonant with an OH−M transition, the population in the lowest level of the ground state decreased. This depletion was monitored with the *probe* laser which was *fixed* on an OH−M transition from the lowest intermolecular level of the ground state to a specific intermolecular vibrational level correlating with OH A $^2\Sigma^+$ ($v' = 1$) + M. Thus, only 0−0 transitions that simultaneously cause a depletion in the OH−M 1−0 LIF signal will be detected. The FD spectra were then obtained by recording the intensity of the fluorescence induced by the probe laser as a function of pump laser wavelength. The details of the normalization procedure and data acquisition have been reported previously.[11,12]

IV. Spectroscopic Results

A. OH−H_2. The fluorescence excitation spectrum observed for OH−H_2 in the OH A−X 1−0 region is shown in Figure 4 (top). The spectrum consists of at least nine broad and, in some cases, overlapping features ascribed to photoexcitation of binary OH−H_2 complexes to various intermolecular vibrational levels correlating with OH A $^2\Sigma^+$ ($v' = 1$) + H_2.[10] The OH−H_2 spectrum spans more than 515 cm^{-1} from 34 968 to 35 483 cm^{-1}. The OH−H_2 features observed in the OH A−X 1−0 spectral region are dramatically broadened as detailed in section VI.A. The intensity of the LIF spectrum builds up while the spacings between the features decrease with increasing excitation wave number. A dramatic cutoff in signal intensity begins at approximately 35 483 cm^{-1}, ∼54 cm^{-1} to higher energy of the OH A−X 1−0 $P_1(1)$ line at 35 429.1 cm^{-1},[43] and returns to baseline by 35 510 cm^{-1}. This drop off in signal intensity is attributed to excitation of OH−H_2 above the OH A $^2\Sigma^+$ ($v' = 1$) + H_2 dissociation limit. The sharp lines superimposed on top of the OH−H_2 signal arise from rotational lines of the OH monomer on the A−X 1−0 transition.

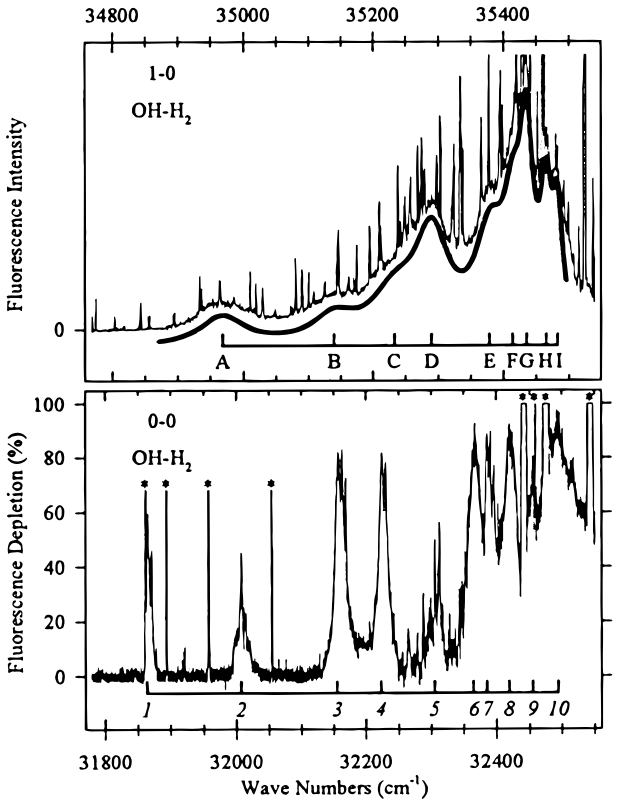

Figure 4. Laser-induced fluorescence (top) and fluorescence depletion (bottom) spectra of OH−H_2 entrance channel complexes recorded in the OH A $^2\Sigma^+$−X $^2\Pi$ 1−0 and 0−0 spectral regions, respectively. The broadened features in both spectra are attributed to excitation of binary OH−H_2 complexes to various intermolecular levels correlating with OH A ($v' = 1$) + H_2 (top) and OH A ($v' = 0$) + H_2 (bottom); sharp lines are OH monomer lines (marked with *'s in the 0−0 spectrum). Displaced below the 1−0 spectrum is a simulation (bold line) which was used to extract the positions, intensities, and homogeneous linewidths of the OH−H_2 features.

A search has been made for the corresponding OH−H_2 features in the OH A−X 0−0 region using LIF.[10,11] In scans covering more than 900 cm^{-1} toward lower energy of the OH A−X 0−0 $P_1(1)$ line at 32 440.6 cm^{-1}, no signals were detected that could be ascribed to electronic transitions of OH−H_2. This indicates that the nonradiative decay processes of quenching and/or reaction depicted in Figure 1 must be occurring on a significantly faster time scale than radiative decay of the complex itself (assumed equal to the OH A $^2\Sigma^+$ radiative lifetime,[44] ∼700 ns). As a result, fluorescence depletion experiments, which provide information analogous to direct absorption measurements, were carried out to investigate the intermolecular vibrational levels derived from OH A $^2\Sigma^+$ ($v' = 0$) + H_2.

The OH−H_2 FD spectrum recorded in the OH A−X 0−0 region (with the probe laser fixed on feature H at 35 465 cm^{-1}) is shown in Figure 4 (bottom). To facilitate comparison of the FD and LIF spectra, the OH−H_2 FD spectrum is plotted as percent fluorescence depletion versus pump laser wave number, in contrast to previously published spectra.[11] In addition, the 0−0 FD and 1−0 LIF spectra have been aligned to account for the OH A $^2\Sigma^+$ $v' = 0 \rightarrow 1$ spacing. A 0% depletion indicates no detectable absorption of OH−H_2/D_2 at a given pump laser wavelength. Most OH lines are not observed in the OH−H_2 FD spectrum; only those intense OH monomer lines that overload the detection electronics appear as narrow peaks and are marked with asterisks.

The OH−H_2 FD spectrum spans more than 700 cm^{-1}, with the lowest observable feature appearing at 31 864 cm^{-1}. At least 10 depletion features have been observed which are due to promotion of OH−H_2 from its ground state to various intermolecular levels correlating with OH A $^2\Sigma^+$ ($v' = 0$) + H_2. As shown in Figure 4, the spacings between OH−H_2 features in the 0−0 FD spectrum (bottom) are similar to those observed in the 1−0 LIF spectrum (top). The breadths of the FD features are significantly narrower than seen in the 1−0 LIF spectrum (see section VI.B). Nearly identical FD spectra were obtained with the probe laser fixed on several different OH−H_2 transitions in the OH A−X 1−0 region. This demonstrates that the extensively broadened OH−H_2 features observed in the 1−0 LIF spectrum originate from the same ground-state level as the narrower FD features seen in the 0−0 region.

The FD spectrum continues beyond feature 10, but at these excitation energies the depletion is nearly continuous with some broad structure superimposed. An LIF scan in this same region reveals a sharp onset of OH−H_2 signal at 32 494.4 cm^{-1}, 53.8 cm^{-1} beyond the OH A−X 0−0 $P_1(1)$ line. This sudden onset is associated with promotion of OH−H_2 above the OH A $^2\Sigma^+$ ($v' = 0$, $n' = 0$) + H_2 dissociation limit via bound → free excitation of transitions to short-lived predissociative resonances of OH−H_2. This will be followed by either direct dissociation or predissociation, yielding fluorescence from the OH A $^2\Sigma^+$ ($v' = 0$, $n' = 0$) fragments and thereby enabling detection via LIF.

B. OH−D_2. The LIF and FD experiments were then repeated with a deuterium carrier gas mixture as a means of confirming the assignment of the OH−H_2 spectra. The LIF spectrum observed in the OH A−X 1−0 spectral region[10] consists of at least 10 broadened features between 34 770 and 35 462 cm^{-1} arising from excitation of OH−D_2 to intermolecular vibrational levels derived from OH A $^2\Sigma^+$ ($v' = 1$) + D_2. The OH−D_2 features appear at distinctly different transition wave numbers than seen for OH−H_2, as expected upon isotopic substitution. The OH−D_2 LIF spectrum exhibits narrower peak widths with less overlap between adjacent features than observed for OH−H_2. The OH−D_2 spectrum exhibits a gradual drop-off in signal beginning near 35 495 cm^{-1}, approximately 66 cm^{-1} beyond the OH A−X 1−0 $P_1(1)$ line. Again, the drop-off is attributed to excitation of the OH−D_2 complex above the OH A $^2\Sigma^+$ ($v' = 1$) + D_2 dissociation limit.

Fluorescence excitation scans of OH−D_2 were also carried out in the OH A−X 0−0 spectral region. Transitions to bound states correlating with OH A $^2\Sigma^+$ ($v' = 0$) + D_2 could not be detected by this method, once again indicating that the nonradiative channels of electronic quenching and/or chemical reaction proceed much more rapidly than radiative decay of the electronically excited complex. An onset of OH−D_2 LIF signal was observed near 32 507 cm^{-1}, approximately 66 cm^{-1} above the OH A−X 0−0 $P_1(1)$ line, which provides a lower limit for the OH A $^2\Sigma^+$ ($v' = 0$, $n' = 0$) + D_2 dissociation limit.

Applying the fluorescence depletion method in the OH A−X 0−0 region (with the probe laser fixed on an OH−D_2 feature in the 1−0 region) revealed a depletion spectrum extending over an even broader energy range than observed for OH−H_2, spanning from 31 803 cm^{-1} to beyond 32 550 cm^{-1}.[11] At least 12 features were observed which are assigned as electronic transitions of OH−D_2 from its ground state to intermolecular levels supported by the OH A $^2\Sigma^+$ ($v' = 0$) + D_2 potential. Again, the OH−D_2 FD features in the 0−0 region were substantially narrower than seen in the 1−0 LIF spectra. In general, the OH−D_2 FD spectrum was analogous to that observed for OH−H_2 in terms of the number of depletions and the overall intensity profile; the positions and energy spacings

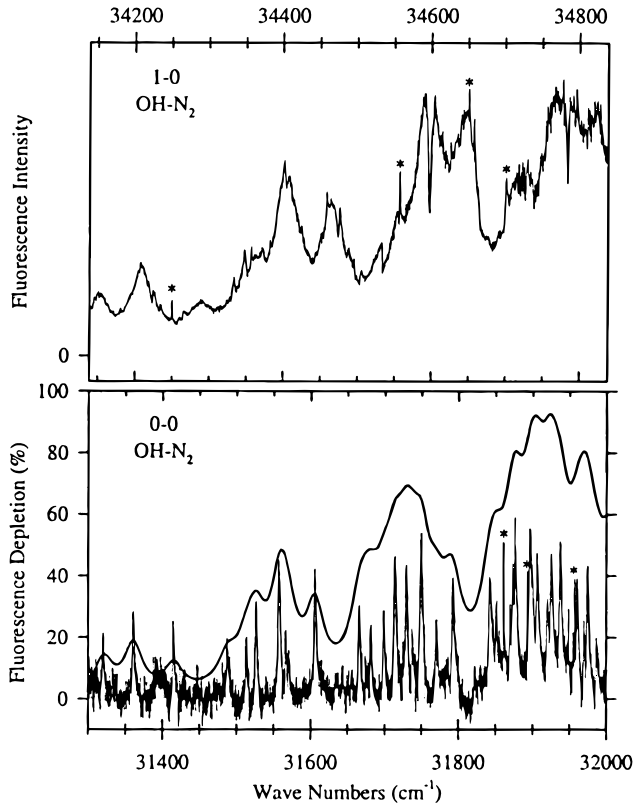

Figure 5. Laser-induced fluorescence (top) and fluorescence depletion (bottom) spectra of OH−N_2 complexes recorded in the OH A $^2\Sigma^+$−X $^2\Pi$ 1−0 and 0−0 spectral regions, respectively. The broadened features in both spectra are attributed to excitation of binary OH−N_2 complexes to various intermolecular levels correlating with OH A ($v' = 1$) + N_2 (top) and OH A ($v' = 0$) + N_2 (bottom); the sharp lines, marked with *'s in both spectra, are OH monomer lines. The lowest energy features in each spectral region have been aligned to facilitate comparison. Also shown in the lower panel is a simulation, where the 0−0 spectrum was homogenously broadened using a 30 cm^{-1} linewidth, that qualitatively reproduces the broad features and underlying background observed for OH−N_2 in the OH A−X 1−0 region.

of the features, however, were distinctly different for OH−D_2 as compared to OH−H_2.

C. OH−N_2. The LIF spectrum of OH−N_2 in the OH A−X 1−0 region spans a 1549 cm^{-1} range from 34 169 to 35 718 cm^{-1}.[9,12] A portion of this spectrum is displayed in the top panel of Figure 5. The broad features and even broader underlying background are attributed to excitation of OH−N_2 to various intermolecular levels supported by the OH A $^2\Sigma^+$ ($v' = 1$) + N_2 potential; sharp lines marked with *'s are due to OH.

Laser-induced fluorescence scans of OH−N_2 have also been performed in the OH A−X 0−0 region. Like both OH−H_2 and OH−D_2, no features attributed to the excitation of OH−N_2 to bound states correlating with OH A $^2\Sigma^+$ ($v' = 0$) + N_2 were detected, presumably due to rapid electronic quenching of OH A $^2\Sigma^+$ by its N_2 partner. A "turn on" of OH−N_2 LIF signal, similar to those seen for OH−H_2 and OH−D_2, was observed beyond 32 692 cm^{-1}, ~251 cm^{-1} above the OH A−X 0−0 $P_1(1)$ line. Again, the onset of LIF identifies the position of the OH A $^2\Sigma^+$ ($v' = 0$) + N_2 dissociation limit.

Fluorescence depletion studies have been carried out to characterize the bound states supported by the OH A $^2\Sigma^+$ ($v' = 0$) + N_2 potential.[12] The OH−N_2 FD spectrum consists of at least 95 features over a 1387 cm^{-1} range from 31 320 to 32 707 cm^{-1}; a portion of the FD spectrum in the OH 0−0 region (recorded with the probe laser at 35 654 cm^{-1}) is shown in the lower panel of Figure 5. To facilitate comparison of the 1−0 and 0−0 spectral regions, the three lowest energy features in the 0−0 FD spectrum (lower panel) have been aligned with the corresponding peaks in the 1−0 LIF spectrum (upper panel). This accounts for the OH A $^2\Sigma^+$ $v' = 0 \rightarrow 1$ spacing and the change in OH−N_2 binding energy upon OH vibrational excitation.

Figure 5 reveals that most of the features in the 1−0 LIF spectrum (top panel) span an energy range that encompasses transitions to several closely spaced OH−N_2 levels derived from OH A $^2\Sigma^+$ ($v' = 0$) + N_2 (bottom panel). Only the three lowest wavenumber features in the 1−0 region can be associated with transitions to single intermolecular levels supported by the OH A $^2\Sigma^+$ ($v' = 0$) + N_2 potential. The homogeneous broadening in the OH−N_2 spectrum is much more extensive in the OH A−X 1−0 region than in the 0−0 region, as resolvable features in the 0−0 region blend together forming broad clumps in the 1−0 spectral region. The magnitude of this broadening in the 1−0 region is estimated in section VI.B.

D. Dispersed Fluorescence Experiments. To determine the source of the fluorescence emission observed following excitation of OH−H_2 and OH−N_2 in the OH A−X 1−0 spectral region, the emission was dispersed with a 0.25 m monochromator.[9,10] The excitation step prepares OH−M complexes with one quantum of OH stretching excitation in the A $^2\Sigma^+$ electronic state. As depicted in Figure 1, these complexes may decay via electronic quenching and/or reaction, vibrational predissociation, and/or radiative decay of the complex itself. Emission was observed exclusively in the OH A−X 0−0 region and *not* in the 1−0 or 1−1 regions that would be indicative of radiative decay of the complex. Since the quenching/reaction channels are dark, the emission in the OH A−X 0−0 region can only originate from the OH A $^2\Sigma^+$ ($v' = 0$) products of vibrational predissociation. This demonstrates that the time scale for vibrational predissociation is much faster than the 700 ns radiative decay of the OH−H_2 or OH−N_2 excited-state complexes (assumed equal to the OH A $^2\Sigma^+$ radiative lifetime[44]). Thus, it is the vibrational predissociation channel that enables the indirect detection of OH−M by LIF in the OH A−X 1−0 spectral region. This channel is energetically closed for OH−M complexes prepared in the OH A $^2\Sigma^+$ electronic state with zero quanta of OH stretch.

V. Binding Energies

The experimental binding energies for H_2, D_2, and N_2 with ground-state OH X $^2\Pi$ can be evaluated from the spectroscopic data in a straightforward manner. The excitation wavenumber which promotes OH−M from its lowest level in the ground state to the OH A $^2\Sigma^+$ ($v' = 0$) + M asymptote, determined from the onset of LIF signal in the OH A−X 0−0 region, must equal the sum of the ground-state binding energy D_0'' and the transition wavenumber of the OH A−X 0−0 $P_1(1)$ line, 32 440.6 cm^{-1}. Ground-state binding energies of 54, 66, and 253 cm^{-1} are determined in this manner for H_2, D_2, and N_2 complexes with OH X $^2\Pi$.[11,12]

Theoretical binding energies have been predicted for OH X $^2\Pi$ with *para*- and *ortho*-H_2 using several different ab initio potentials;[14,16] analogous calculations have not yet been carried out for OH X $^2\Pi$ with D_2 or N_2. The theoretical calculations indicate that the spherically symmetric *para*-H_2 ($j = 0$) will be far less well bound to OH X $^2\Pi$ than the dumbbell-shaped *ortho*-H_2 ($j = 1$); thus, the experimental spectra are presumed to be due to the *ortho*-H_2 complex. Also, nuclear spin statistics favor *ortho*-H_2 over *para*-H_2 by a 3:1 population ratio.[45] Recently, the rotationally resolved infrared overtone spectrum of the

ground electronic state of OH−H_2 has been observed,[46] confirming that the experimental spectra are due to *ortho*-H_2−OH. The experimentally determined D_0'', 54 cm^{-1}, for OH−H_2 compares favorably with the value predicted theoretically for complexes of OH X $^2\Pi$ with *ortho*-H_2, 42 cm^{-1}, based on the MCKW potential.[16] The binding energy is quite small compared to the well depth at the T-shaped O−H--H_2 minimum energy configuration (188 cm^{-1}) as a result of the large zero-point energy that arises from the small reduced mass, large monomer rotational constants, and sizable anisotropy of the potential.[16]

For OH in its excited A $^2\Sigma^+$ electronic state, lower limits on its binding energies with H_2, D_2, and N_2 can also be determined directly from the experimental spectra. The OH A $^2\Sigma^+$ ($v' = 0$) + M bond energy is deduced from the span of the FD spectra in the OH A−X 0−0 region with respect to the OH A $^2\Sigma^+$ ($v' = 0$) + M asymptote. This yields lower limits for the bond energies of OH A $^2\Sigma^+$ ($v' = 0$) with M = H_2, D_2, and N_2 of 631, 704, and 1372 cm^{-1}, respectively.[11,12] The binding energy of the molecular partner to OH A $^2\Sigma^+$ ($v' = 1$) is evident from the range of the LIF spectra in the OH A−X 1−0 region with respect to the OH A $^2\Sigma^+$ ($v' = 1$) + M dissociation limit. This gives lower limits of 515, 725, and 1511 cm^{-1} for the binding energies of OH A $^2\Sigma^+$ ($v' = 1$) to H_2, D_2, and N_2, respectively.[11,12]

The experimental binding energies of OH−H_2 and OH−D_2 are found to increase by at least an order of magnitude upon electronic excitation of the OH moiety, while for OH−N_2 the increase is more than 5-fold. These changes are in accord with ab initio calculations of the intermolecular potentials for OH in its ground X $^2\Pi$ and excited A $^2\Sigma^+$ electronic states with H_2 and N_2.[16,17] The well depth in the minimum energy configuration (T-shaped for OH−H_2/D_2, collinear for OH−N_2) is predicted to increase from 188 to 2900 cm^{-1} for H_2/D_2 and from 460 to 3770 cm^{-1} for N_2 upon electronic excitation of OH.

Hernández and Clary[38,47] have computed the intermolecular vibrational levels supported by the OH A $^2\Sigma^+$ + H_2/D_2 potentials; analogous calculations are still needed for OH A $^2\Sigma^+$ + N_2. The orthogonal modes for OH−H_2/D_2 consist of the pure intermolecular stretch, two in-plane asymmetric bending motions of the three hydrogen atoms, and an out-of-plane bend of the three hydrogen atoms. These vibrational motions give rise to an extremely large zero-point energy that amounts to ∼50% of the well depth. The theoretical predictions provide a valuable template of the intermolecular vibrational level pattern that has been used as a guide in assigning the experimentally observed features. The experimentally observed OH−H_2 intermolecular vibrational levels associated with OH A $^2\Sigma^+$ v' = 0 (displayed in Figure 2) and $v' = 1$, however, are significantly less well bound than the lowest level predicted by theory, suggesting that the lowest intermolecular levels supported by the OH A $^2\Sigma^+$ + H_2 potentials have not been experimentally observed. This is not surprising since the OH−H_2 equilibrium intermolecular bond length decreases by ∼1.0 Å upon electronic excitation of OH, as shown in Figure 2. This will result in poor Franck−Condon overlap and thus weak intensity for transitions to intermolecular levels lying low in the A-state well. In fact, Hernández and Clary[38] have predicted that the intensity for the electronic transition to the lowest intermolecular level supported by the OH A $^2\Sigma^+$ + H_2 potential will be at least an order of magnitude weaker than that for the first excited stretching level. Similarly, the lowest intermolecular levels correlating with OH A $^2\Sigma^+$ + D_2 are probably not detected as a result of poor Franck−Condon overlap.

An analogous situation is expected for OH−N_2, where the intermolecular bond length is predicted to decrease by ∼0.9 Å upon electronic excitation of OH.[18] This will result in optimum Franck−Condon overlap to levels lying closest to the OH A $^2\Sigma^+$ + N_2 dissociation limit and weaker intensity of transitions to intermolecular levels positioned deeper in the well. Indeed, only intermolecular levels lying in the upper 40% of the attractive well have been detected by LIF or FD methods, as illustrated in Figure 3.

VI. Excited-State Lifetimes

A. OH A $^2\Sigma^+$ ($v' = 0$) + M. Many of the OH−H_2, D_2, and N_2 features observed via FD in the OH A−X 0−0 spectral region exhibit partial rotational band structure. The magnitudes of the depletions for OH−H_2/D_2 and OH−N_2 were quite large—up to 80%—at the pump laser pulse energies (∼25 mJ/pulse) used to record Figures 4 and 5 (bottom). The pump laser power and associated depletions were significantly reduced in order to record FD spectra suitable for rotational contour analysis. A pulse energy of 0.3 mJ/pulse was the lowest pump laser power for which a modest signal-to-noise level could be achieved for features in the OH−H_2 and OH−D_2 spectra, while 2 mJ/pulse was the lower limit for OH−N_2. At the lowest pulse energies, the contribution of saturation broadening was minimized, permitting the excited-state lifetimes of the complexes (lower limits) to be derived from the homogeneous component of the linewidth.

The homogeneous linewidths of the features were extracted via a rotational contour least-squares fitting procedure.[11] To simulate the rotational structure, several assumptions had to be made. The OH−M rotational structure was computed using a pseudodiatomic model, (OH)···M, a rotational temperature of ∼3K, and ground-state rotor constants of 0.75, 0.5, and 0.12 cm^{-1} for OH−H_2, D_2, and N_2, respectively.[16,48,49] The band origin, excited-state rotor constant, and homogeneous (Lorentzian) component of the linewidth were allowed to vary in the fitting procedure. Additionally, the intensities have been fit by assuming parallel and perpendicular transition types; both yielded comparable homogeneous linewidths.

The OH−H_2 FD features exhibit homogeneous linewidths ranging from 1.2 to 1.7 cm^{-1}. The corresponding lifetimes of the intermolecular vibrational levels accessed by electronic spectroscopy range from 4.5 to 3.2 ps. The OH−D_2 bands that could be analyzed (adequate signal-to-noise level and spectrally isolated) yielded linewidths of approximately 1.2 cm^{-1} and corresponding excited-state lifetimes of 4.5 ps. In Figure 6, the resultant OH−H_2/D_2 linewidths and corresponding lifetimes are plotted on a logarithmic scale versus the position of the excited-state level relative to the OH A $^2\Sigma^+$ ($v' = 0$) + H_2/D_2 asymptote. These values represent upper limits for the magnitude of lifetime broadening and, therefore, lower limits for the lifetimes of complexes prepared in the intermolecular vibrational levels due to the possibility of saturation broadening even at these reduced laser powers.

The homogeneous linewidths of the OH−N_2 features were extracted using the same least-squares fitting procedure.[12] Lorentzian linewidths of 0.7−3.9 cm^{-1} have been determined for OH−N_2 features that are well isolated from others and have adequate signal-to-noise levels, specifically 16 features between 31 320 and 32 362 cm^{-1}. The linewidths indicate that OH−N_2 complexes prepared in the corresponding levels derived from OH A $^2\Sigma^+$ ($v' = 0$) + N_2 have lifetimes ranging from 1.4 to 8 ps; these values represent lower limits due to residual saturation broadening.

The line broadening observed in the OH−H_2, OH−D_2, and OH−N_2 0−0 FD spectra can also be used to estimate the

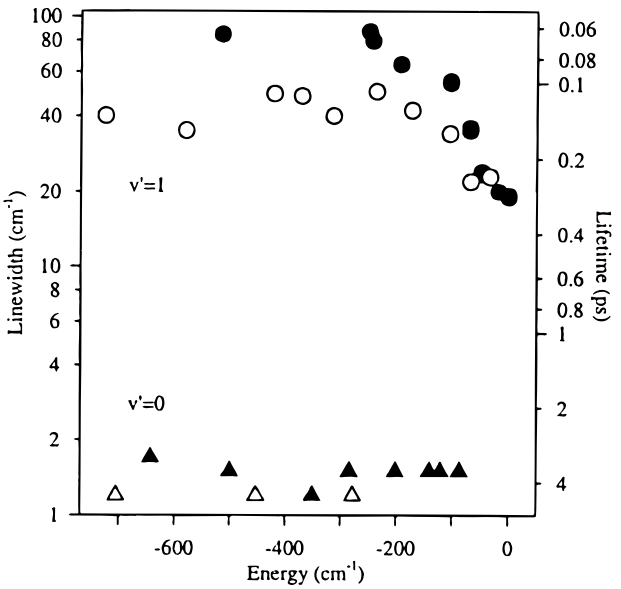

Figure 6. The OH−H_2 and OH−D_2 homogeneous linewidths and corresponding lifetimes plotted as filled and open symbols, respectively, on a logarithmic scale with the abscissa representing the energy by which each excited-state level is bound. The values indicated as circles correspond to those features that are associated with the OH A $^2\Sigma^+$ ($v' = 1$) + H_2/D_2 asymptote, while the triangles correlate with the OH A $^2\Sigma^+$ ($v' = 0$) + H_2/D_2 asymptote. The reported linewidths represent upper limits, while the lifetimes are lower limits due to the possibility of saturation broadening of the spectral features.

fluorescence quantum yield, Φ, for OH−M complexes prepared in intermolecular levels derived from OH A $^2\Sigma^+$ ($v' = 0$) + M.[11,12] Φ is given by the radiative decay rate, $(\tau_{rad})^{-1}$, divided by the total decay rate, $(\tau_0)^{-1}$. Using the values (lower limits) determined experimentally for τ_0, 3.2−4.5 ps for OH−H_2/D_2 and 1.4−8 ps for OH−N_2, and assuming that the radiative lifetime for OH−M is equal to that for OH ($\tau_{rad} \approx 700$ ns),[44] results in fluorescence quantum yields on the order of 10^{-6}. This value is consistent with the inability to detect OH−H_2, OH−D_2, or OH−N_2 transitions in the OH A−X 0−0 region by LIF.

B. OH A $^2\Sigma^+$ ($v' = 1$) + M. The OH−H_2/D_2 features observed in the OH A−X 1−0 spectral region are substantially broader than those seen in the 0−0 region and do not exhibit resolvable rotational structure. This is clearly seen in Figure 4 for OH−H_2, where the 1−0 LIF spectrum (top) is compared with the 0−0 FD spectrum (bottom). The breadths of the OH−H_2/D_2 1−0 LIF features were unchanged as the laser pulse energy was reduced from 30 mJ to 5 mJ, the lowest pulse energy for which these spectra could be readily observed. This demonstrates that saturation broadening is not a significant source of line broadening in the spectra.

The breadths of the OH−H_2/D_2 features observed in the OH A−X 1−0 region are far greater than the inhomogeneous rotational band structure anticipated from analysis of the corresponding 0−0 features and ab initio predictions.[16,38] As a result, all of the OH−H_2/D_2 intermolecular vibrational features were fit to simple Lorentzians in order to extract their peak positions, relative intensities, and homogeneous linewidths. The resultant fit of the OH−H_2 features is shown (bold line) below the experimental data in Figure 4 (top); the tic marks in Figure 4 (top) identify the positions of the OH−H_2 features.

The Lorentzian linewidths extracted from the LIF spectra vary from 19 to 87 cm^{-1} for OH−H_2 and from 22 to 50 cm^{-1} for OH−D_2. The corresponding lifetimes for the excited-state levels derived from OH A $^2\Sigma^+$ ($v' = 1$) + H_2/D_2 are approximately 60−280 fs and 110−240 fs, respectively. The OH−D_2 complexes are longer lived, by roughly a factor of 2, than OH−H_2 complexes with a similar degree of intermolecular excitation until near the OH A $^2\Sigma^+$ ($v' = 1$) + H_2/D_2 asymptote, where the lifetimes become comparable (see Figure 6). Both the H_2 and D_2 complexes exhibit a trend of decreasing linewidth (increasing lifetime) with increasing excitation energy. As shown in Figure 6, the $v' = 1$ lifetimes are a factor of 10−75 times shorter than observed for the intermolecular levels correlating with OH A $^2\Sigma^+$ ($v' = 0$) + H_2/D_2.

The decrease in lifetime upon OH A $^2\Sigma^+$ $v' = 0 \rightarrow 1$ vibrational excitation cannot simply be attributed to the addition of the vibrational predissociation channel. Rather, ab initio calculations show that the OH A $^2\Sigma^+$ + H_2 potential depends strongly on the O−H internuclear distance as a result of a significant amount of interaction between the three hydrogen atoms.[17,38] This suggests that OH vibrational excitation may enhance the rate of electronic quenching and/or chemical reaction. The origins of these nonradiative decay channels are discussed in section VII.B.

For OH−N_2, the homogeneous broadening in the 1−0 spectral region is far more extensive than observed in the 0−0 region (Figure 5). If a similar number and pattern of intermolecular energy levels correlate with OH A $^2\Sigma^+$ ($v' = 0$) + N_2 and OH A $^2\Sigma^+$ ($v' = 1$) + N_2, as found for analogous systems (e.g., OH−Ar, OH−H_2), then the primary reason for the dramatic change in the appearance of the OH−N_2 spectra between the OH A−X 0−0 and 1−0 regions can be attributed to homogeneous line broadening. The magnitude of the homogeneous broadening in the 1−0 spectrum has been estimated through simulations based on the experimental 0−0 spectrum with various broadening terms. The homogeneous linewidth was varied until the simulation qualitatively resembled the experimental 1−0 spectrum. The best agreement has been obtained with a Lorentzian linewidth of 30 cm^{-1}, which yields the simulated spectrum shown in the bottom panel of Figure 5 (bottom).

A linewidth of 30 cm^{-1} corresponds to a lifetime of ∼180 fs for OH−N_2 complexes prepared with one quantum of vibrational excitation in the excited electronic state. This can be compared to lifetimes ranging between 1.4 and 8 ps (lower limits) for levels correlating to OH A $^2\Sigma^+$ ($v' = 0$) + N_2. Thus, OH−N_2 prepared in intermolecular levels derived from OH A $^2\Sigma^+$ ($v' = 1$) decay some 25 times faster than in levels associated with $v' = 0$. Again, ab initio calculations indicate that the O−H bond is coupled to the intermolecular coordinates,[18] suggesting that OH A $^2\Sigma^+$ vibrational excitation may enhance the rate of quenching as well as open the vibrational predissociation channel. The origins of the homogeneous broadening and exceedingly short excited-state lifetimes will be discussed in section VII.C.

VII. Origins of Quenching

The homogeneous line broadening evident in the electronic spectra of OH−M complexes, the low fluorescence quantum yield for OH−M complexes prepared in intermolecular levels derived from OH A $^2\Sigma^+$ ($v' = 0$) + M, and the significant cross sections for removal of OH from the A $^2\Sigma^+$ ($v' = 0$) electronic state upon collisions[20−26] with M = H_2, D_2, or N_2 indicate that the nonradiative processes of electronic quenching and/or chemical reaction are occurring in these systems. The ab initio calculations of Clary, Werner, and co-workers pointed to specific regions of the OH A $^2\Sigma^+$ + H_2 potential energy surface that may be responsible for quenching and/or reaction.[16] Specifically, they noted that the excited-state complex should only be metastable since the T-shaped H−O--H_2 and linear H−O--H−H

structures could result in reaction to $H_2O + H$. These "reactive" channels, however, appeared to be separated by relatively high barriers from the potential minimum in the T-shaped O−H--H_2 structure. In addition, Hernández and Clary found that the harmonic frequency for the bending mode of OH−H_2 in its excited electronic state became imaginary in the short-range region of the potential (at energies well below the dissociation limit), providing a low-energy path for the formation of $H_2O + H$ products.[38] A saddle point for this process was found in the vicinity of the dissociation limit in the work of Kliesch.[50] Recently, more comprehensive ab initio calculations have been carried out to identify the pathways for these decay processes in the OH + H_2 and OH + N_2 systems and are presented here; details of these calculations will be published elsewhere.[17,18]

A. Ab Initio Methods. The ab initio calculations[17,18] use the complete active space self consistent field (CASSCF)/internally contracted configuration interaction (ICCI) methods as implemented in MOLPRO.[51,52] The basis sets are the correlation consistent basis sets of Dunning.[53] For OH + H_2 the cc-pVQZ basis set was used minus the f functions on H, and this basis set was augmented by one set of diffuse spd functions on oxygen and one set of diffuse sp functions on H. Thus, this basis set is denoted as aug-cc-pVQZ′ (where the prime denotes that the f functions on H were omitted). For OH + N_2 the aug-cc-pVTZ and aug cc-pVQZ basis sets were used. In general, the CASSCF active spaces included all electrons except the O 1s and O 2s in the case of OH + H_2 and the O 1s, O 2s and N 1s, N 2s in the case of OH + N_2. The reference space for the subsequent ICCI calculations was the CASSCF wave function for the OH + H_2 calculations and was a selected reference space with a threshold on CI coefficient in the CASSCF wave function of 0.05 for the OH + N_2 calculations.

B. Quenching of OH A $^2\Sigma^+$ by H_2. The interaction energy between electronically excited OH A $^2\Sigma^+$ and H_2 has been computed for specific orientations and separation distances while holding the OH and H_2 bond lengths fixed. The minimum energy configuration was found to be T-shaped with the hydroxyl hydrogen pointing toward the center of the hydrogen molecule, as had been determined in earlier ab initio calculations.[16] The energy was further minimized by allowing the internuclear distances of the OH and H_2 moieties to change as the intermolecular separation was varied in fixed geometries.[17,38] The resultant potential has a well depth of ∼2900 cm^{-1} at an equilibrium separation distance of 2.1 Å in the T-shaped O−H--H_2 minimum energy configuration.[16,37] The minimum energy path for OH A $^2\Sigma^+$ + H_2 in this configuration is shown in Figure 7 (filled circles). At the minimum energy location, the H_2 bond length is increased by 5% and that of OH by 4% from their corresponding values in the separated molecule limit. These increases in the monomer bond lengths suggest that the H_2 and OH vibrations are coupled to the intermolecular degrees of freedom. Also displayed in Figure 7 is a radial cut of the ab initio potential (open circles) for the T-shaped H−O--H_2 geometry; that is, with the OH radical rotated by 180° from its minimum energy configuration.

The ab initio calculations of the ground-state OH X $^2\Pi$ + H_2 potentials have also been extended to shorter intermolecular distances and, therefore, higher energies on the repulsive wall.[16,17] Two potentials correlate with OH X $^2\Pi$ + H_2, the A′ and A″ surfaces, depending on the orientation of the orbital containing the unpaired electron of OH with respect to the OH−H_2 plane. Radial cuts of the A′ surface, with the orbital of the unpaired electron lying in plane, are illustrated in Figure 7 for the T-shaped O−H--H_2 (filled circles) and H−O--H_2 (open circles) configurations.

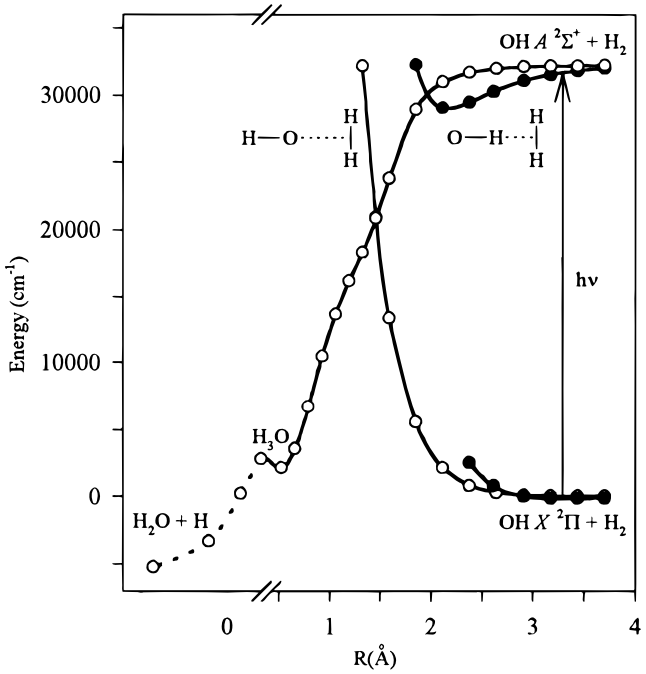

Figure 7. Ab initio calculations of the interaction energy for molecular hydrogen with ground OH X $^2\Pi$ and electronically excited OH A $^2\Sigma^+$ radicals in the T-shaped O−H--H_2 (filled circles) and H−O--H_2 (open circles) configurations at specific intermolecular separation distances, *R*. The ground- and excited-state surfaces of A′ symmetry intersect more than 11 000 cm^{-1} below the OH A $^2\Sigma^+$ + H_2 asymptote in the T-shaped H−O--H_2 configuration. Two pathways exit from the conical intersection: the electronic quenching pathway follows down to ground-state OH X $^2\Pi$ + H_2, and the reaction pathway generates $H_2O + H$ after passing through the H_3O intermediate. The dashed line and break in the abscissa indicate that this axis has changed to a reaction coordinate. Electronic excitation ($h\nu$) of OH−H_2 complexes accesses intermolecular vibrational levels in which the OH and H_2 moieties undergo large-amplitude motions about the O−H--H_2 minimum energy structure. Electronic quenching and/or reaction proceeds via the conical intersection in the H−O--H_2 configuration. Figure adapted from ref 17.

The ground- and excited-state potentials, both of A′ symmetry in planar geometries, intersect as shown in Figure 7 for the T-shaped H−O--H_2 configuration. This conical intersection lies more than 11 000 cm^{-1} below the OH A $^2\Sigma^+$ + H_2 asymptote (and greater than 20 000 cm^{-1} above the OH X $^2\Pi$ + H_2 asymptote) at an intermolecular separation distance of ∼1.4 Å. The nuclear configurations representing a circular path around the cone of the OH_3 conical intersection are depicted by Yarkony in Figure 7 of ref 19. There are two pathways that can be followed after leaving the conical intersection: electronic quenching and chemical reaction. The electronic quenching pathway follows down to the OH X $^2\Pi$ + H_2 asymptote in the H−O--H_2 configuration, thereby regenerating reactants.

The $H_2O + H$ reaction pathway contains a shallow minimum corresponding to the H_3O intermediate which lies ∼1750 cm^{-1} above the OH X $^2\Pi$ + H_2 asymptote. H_3O has a C_{3V} structure in which the three H atoms lie in a planar equilateral triangle and the O atom is situated in the center of the triangle above the plane of the hydrogen atoms.[54] Converting from the T-shaped H−O--H_2 geometry to H_3O involves structural changes in many different coordinates. The dashed line and break in the abscissa in Figure 7 indicate that this axis has changed from the (OH)--(H_2) intermolecular separation distance, *R*, to a reaction coordinate proceeding from the conical intersection to H_3O and the $H_2O + H$ products.

Thermal collisions of electronically excited OH A $^2\Sigma^+$ radicals with H_2 average over all orientations of the partners. Clearly, some of these collisions will access the specific orientations that lead to electronic quenching and/or chemical reaction. On the other hand, OH−H_2 complexes sample a restricted range of orientations between the OH A $^2\Sigma^+$ and H_2 monomers. Electronic excitation promotes OH−H_2 from its ground state, correlating with OH X $^2\Pi$ + H_2, to specific intermolecular vibrational levels in the excited OH A $^2\Sigma^+$ electronic state (arrow in Figure 7). In the levels probed experimentally, the OH and H_2 subunits undergo large-amplitude bending and intermolecular stretching motions about the T-shaped O−H--H_2 minimum energy structure. For quenching and/or reaction to occur, the OH monomer must access the H−O--H_2 configuration in the excited electronic state (shown in Figure 7) or others that lead to a conical intersection with the ground-state surface. The ab initio calculations of the OH A $^2\Sigma^+$ + H_2 potential show that the barrier to OH internal rotation decreases with increasing intermolecular separation distance, making the conversion plausible at large *R*. The internal rotation of OH involves mainly the motion of a hydrogen atom. Thus, tunneling may contribute significantly to the rate of conversion from O−H--H_2 to H−O--H_2 in the excited electronic state. The rate of this conversion may be enhanced when OH A $^2\Sigma^+$ is vibrationally excited as a result of strong interactions between the three hydrogen atoms.

In $v' = 1$, the experimental lifetimes indicate that quenching/reaction is approximately a factor of 2 slower in OH−D_2 than OH−H_2, possibly as a result of a reduced amplitude for the OH bending motion in the deuterated species. The lifetimes become comparable near the OH A $^2\Sigma^+$ + H_2/D_2 dissociation limit, where the barrier to internal rotation of OH is significantly reduced.[16] In thermal collisions, which access all configurations, the quenching cross sections are similar for OH A $^2\Sigma^+$ ($v' = 0$) with H_2 and D_2.[23]

C. Quenching of OH A $^2\Sigma^+$ by N_2. High-level ab initio calculations have also been carried out to determine the intermolecular interaction energy between N_2 and OH in its ground X $^2\Pi$ and excited A $^2\Sigma^+$ electronic states for selected configurations and intermolecular separation distances.[18] The minimum energy configuration is found to be linear O−H--N≡N in both the ground and excited electronic states. The OH X $^2\Pi$ + N_2 and OH A $^2\Sigma^+$ + N_2 potentials are calculated to have well depths of 460 and 3770 cm^{-1} at intermolecular separation distances of $R = 3.9$ and 3.0 Å, respectively, in this O−H--N≡N geometry. The minimum energy pathways were computed by allowing the OH and N_2 bond lengths to vary. The OH bond length increased by ∼5% and the N≡N bond length was essentially unchanged at the minimum of the excited-state potential in the linear O−H--N≡N configuration. This suggests that the OH stretch will couple efficiently to the intermolecular degrees of freedom.

Radial cuts of the OH X $^2\Pi$ + N_2 and OH A $^2\Sigma^+$ + N_2 minimum energy pathways in the linear O−H--N≡N (filled circles) and H−O--N≡N (open circles) configurations are shown in Figure 8. A secondary minimum has been identified for the OH A $^2\Sigma^+$ + N_2 potential in the collinear H−O--N≡N configuration with a well depth of 2800 cm^{-1} at an intermolecular separation distance of 2.3 Å. The A′ potential derived from the ground state intersects the excited-state curve, also of A′ symmetry, in the vicinity of the secondary minimum in the linear H−O--N≡N configuration. This conical intersection occurs about 2300 cm^{-1} below the OH A $^2\Sigma^+$ + N_2 asymptote. This is presumably the key crossing in the electronic quenching of OH A $^2\Sigma^+$ by N_2, which leads to OH X $^2\Pi$ + N_2 products.

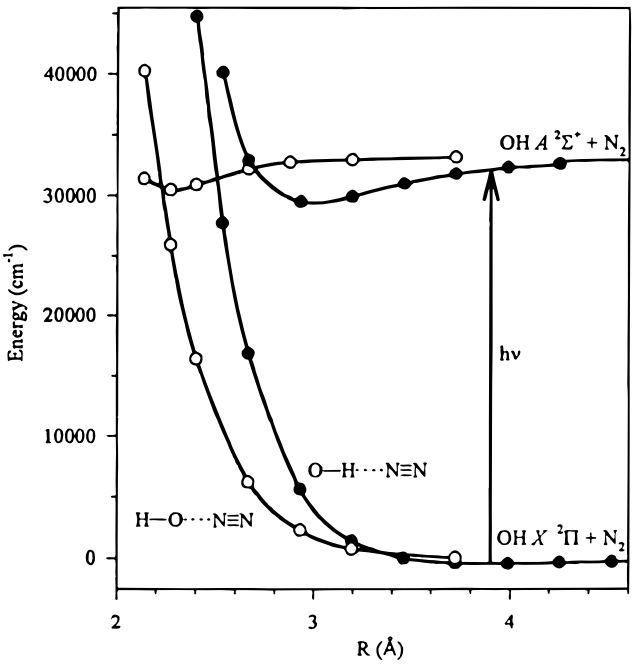

Figure 8. Ab initio interaction energies for N_2 with OH in its ground X $^2\Pi$ and excited A $^2\Sigma^+$ electronic states for the linear O−H--N≡N (filled circles) and H−O--N≡N (open circles) configurations at specific intermolecular separation distances, *R*. In the H−O--N≡N configuration, the ground and excited states intersect ∼2300 cm^{-1} below the OH A $^2\Sigma^+$ + N_2 asymptote, giving rise to electronic quenching. OH−N_2 complexes, stabilized in a shallow minimum about the O−H--N≡N configuration in the ground electronic state, are promoted to the OH A $^2\Sigma^+$ electronic state ($h\nu$). Wide amplitude OH bending motion presumably provides access to H−O--N≡N and/or other configurations that lead to quenching. Figure adapted from ref 18.

Additional conical intersections have been identified for collinear O−H--N≡N and for H−O--N_2 in a T-shaped configuration with the oxygen of the hydroxyl radical pointing towards the center of the N_2 bond. These conical intersections occur significantly above the OH A $^2\Sigma^+$ + N_2 asymptote (>1000 cm^{-1} in the T-shaped configuration and 10-fold higher for collinear O−H--N≡N) and, therefore, are not likely to be important for quenching in complexes or in thermal collisions. Finally, pathways to reactive channels, specificially H + N_2O and NH + NO, have not been identified in the ab initio calculations, although these channels are energetically feasible starting from OH A $^2\Sigma^+$ ($v' = 0, 1$) + N_2.[55,56]

Collisions of OH A $^2\Sigma^+$ with N_2 will sample all orientations of the partners, including those that lead to quenching at thermal energies. By contrast, OH−N_2 complexes are promoted from their ground state, with configurations about the linear O−H--N≡N minimum energy structure, to excited intermolecular bending and stretching levels correlating with OH A $^2\Sigma^+$ + N_2 (arrow, Figure 8). For electronically excited OH−N_2 complexes to decay via electronic quenching, the OH monomer must undergo an extremely wide amplitude bending motion to reach the H−O--N≡N configuration or others that lead to a conical intersection with the ground electronic state. This may occur at large intermolecular separation distances, where the barrier to internal rotation of OH is small, or via tunneling through the barrier. For the intermolecular levels of OH A $^2\Sigma^+$ ($v' = 0$) + N_2 observed experimentally, the conversion to H−O--N≡N and subsequent quenching is found to occur on a picosecond time scale. Vibrational excitation of OH results in significantly faster decay via quenching and/or vibrational predissociation as a result of the coupling between the OH and intermolecular vibrations.

VIII. Conclusions and Future Directions

This feature article examines the mechanism for quenching of electronically excited OH A $^2\Sigma^+$ radicals by molecular hydrogen, deuterium, and nitrogen from both experimental and theoretical perspectives. Many of the previous experimental investigations of electronic quenching involved collision studies at thermal energies.[20−26] Recent spectroscopic studies of weakly bound OH−M (M = H_2, D_2, and N_2) complexes have provided a new experimental approach for examining electronic quenching and/or chemical reaction in these systems.[9−12] The origins of electronic quenching have been revealed through ab initio calculations of the OH (A $^2\Sigma^+$, X $^2\Pi$) + M potential energy surfaces, in particular, by identifying the locations of conical intersections between these surfaces.[17,18]

The electronic spectroscopy studies of OH−M complexes have probed many of the intermolecular stretching and bending vibrational levels supported by the OH A $^2\Sigma^+$ ($v' = 0, 1$) + M potentials.[11,12] The experimentally observed levels lie within the upper portions of the deep OH A $^2\Sigma^+$ + M potentials wells, with depths of 2900 cm^{-1} for H_2 and 3770 cm^{-1} for N_2, and extend to the dissociation limits. Comparison of the experimental data with the bound states computed for ab initio intermolecular potential energy surfaces provides a rigorous test of the ab initio potentials. A comparison of this kind has been carried out for OH A $^2\Sigma^+$ + H_2.[38,47] Differences between experiment and theory can lead to refinements of the potential energy surface. Such refinements should now be possible for the OH A $^2\Sigma^+$ + H_2/D_2 and N_2 systems.

Homogeneous line broadening of the OH−H_2, OH−D_2, and OH−N_2 features in the OH A−X 0−0 and 1−0 spectral regions yields the rates for dynamical processes occurring under the restricted geometries sampled by OH−M complexes in various intermolecular levels of the excited electronic state. OH−M complexes prepared in the OH A $^2\Sigma^+$ ($v' = 0$) state decay on a picosecond time scale as a result of electronic quenching and/or chemical reaction. Complexes prepared with one quantum of OH vibrational excitation in the A $^2\Sigma^+$ state decay 10−75 times faster than observed for $v' = 0$ due to electronic quenching and/or reaction, processes that may be accelerated upon OH vibrational excitation, as well as vibrational predissociation.

Ab initio calculations have revealed the OH−M configurations that lead to quenching of OH A $^2\Sigma^+$ by M, namely, T-shaped H−O--H_2 and linear H−O--N≡N. These calculations show that quenching proceeds via a conical intersection between the A′ surfaces correlating with OH (A $^2\Sigma^+$, X $^2\Pi$) + M at energies below the excited-state asymptote. In the OH−H_2 system, two pathways lead away from the conical intersection, one to OH X $^2\Pi$ + H_2 (quenching) and the other to H_2O + H (reaction). The branching ratio and product-state distributions for these processes are not known, but are of great interest due to possible dynamical effects (e.g. geometric phase effect[57]) in passing through the conical intersection region.[19]

Dynamical calculations of the rates for electronic quenching, chemical reaction, and vibrational relaxation under full collision and complex conditions are still needed. A very important aspect of these calculations will be the proper treatment of the conical intersection region.[19] These calculations will test the ab initio potentials and the implicit mechanism for quenching. In addition, the theoretical calculations will be useful in interpreting the experimental findings, particularly for OH−M complexes where the rate-limiting step for quenching/reaction may be internal rotation of OH within the excited-state complex. Hopefully, the results presented here for electronic quenching of OH A $^2\Sigma^+$ by molecular hydrogen and nitrogen, systems of fundamental importance in atmospheric and combustion chemistry, will stimulate such calculations.

In the future, the experimental and theoretical studies of OH A $^2\Sigma^+$ quenching should be extended to other molecular partners to test the generality of the mechanism described here. To date, OH A $^2\Sigma^+$ quenching cross sections have been measured for collision partners such as O_2 and H_2O,[6] which are important for atmospheric monitoring purposes, as well as CO, CO_2, and NO,[30] which are of significance in combustion and aerothermodynamic systems. These partners have not yet been examined in OH complexes. Ab initio potential energy surfaces are also needed for OH (A $^2\Sigma^+$, X $^2\Pi$) with these partners. So far, intermolecular potentials have been calculated for OH (A $^2\Sigma^+$, X $^2\Pi$) + CO,[58,59] which exhibit conical intersections between the ground- and excited-state surfaces for specific orientations of the partners, linear O−C--O−H and O−C--H−O at energies −1.3 and +0.4 eV with respect to the OH A $^2\Sigma^+$ + CO asymptote.[58] In addition, OH A $^2\Sigma^+$ + CO illustrates the rich chemistry that can occur in these systems.[58]

Acknowledgment. The research in the Lester laboratory at the University of Pennsylvania has been sponsored by the Division of Chemical Sciences of the Department of Energy and the National Science Foundation. The authors acknowledge the contributions of present and past members of the Lester group in carrying out and interpreting the OH−H_2/D_2 and OH−N_2 experiments, particularly Leanna C. Giancarlo, R. Timothy Bonn, and Robert W. Randall. R.A.L. also thanks the National Research Council for financial support while writing this feature article. S.P.W. was supported by NASA Contract No. NAS2-14031 to ELORET. The authors thank David C. Clary, Ramón Hernández, and David Yarkony for valuable discussions and sharing the results of their calculations prior to publication.

References and Notes

(1) Wayne, R. P. *Chemistry of Atmospheres: An Introduction to the Chemistry of the Atmospheres of Earth, the Planets, and their Satellites*, 2nd ed.; Oxford University Press: Oxford, 1991.
(2) Graedel, T. E.; Crutzen, P. J. *Atmospheric Change: An Earth System Perspective*; W. H. Freeman: New York, 1993.
(3) Glassman, I. *Combustion*, 2nd ed.; Academic Press, Inc.: Orlando FL, 1987.
(4) Warnatz, J.; Maas, U.; Dibble, R. W. *Combustion: Physical and Chemical Fundamentals, Modelling and Simulation, Experiments, Pollutant Formation*; Springer-Verlag: Berlin Heidelberg, 1996.
(5) Rothe, E. W.; Andresen, P. *Appl. Opt.* **1997**, *36*, 3971.
(6) Crosley, D. R. *J. Phys. Chem.* **1989**, *93*, 6273.
(7) Andresen, P.; Bath, A.; Gröger, W.; Lülf, H. W.; Meijer, G.; ter Meulen, J. J. *Appl. Opt.* **1988**, *27*, 365.
(8) Arnold, A.; Ketterle, W.; Becker, H.; Wolfrum, J. *Appl. Phys. B* **1990**, *51*, 99.
(9) Giancarlo, L. C.; Lester, M. I. *Chem. Phys. Lett.* **1995**, *240*, 1.
(10) Loomis, R. A.; Lester, M. I. *J. Chem. Phys.* **1995**, *103*, 4371.
(11) Loomis, R. A.; Schwartz, R. L.; Lester, M. I. *J. Chem. Phys.* **1996**, *104*, 6984.
(12) Schwartz, R. L.; Giancarlo, L. C.; Loomis, R. A.; Bonn, R. T.; Lester, M. I. *J. Chem. Phys.* **1996**, *105*, 10224.
(13) Kochanski, E.; Flower, D. R. *Chem. Phys.* **1981**, *57*, 217.
(14) Miller, S. M.; Clary, D. C. *J. Chem. Phys.* **1993**, *98*, 1843.
(15) Offer, A. R.; van Hemert, M. C. *J. Chem. Phys.* **1993**, *99*, 3836.
(16) Miller, S. M.; Clary, D. C.; Kliesch, A.; Werner, H. J. *Mol. Phys.* **1994**, *83*, 405.
(17) Walch, S. P. To be published.
(18) Walch, S. P. To be published.
(19) Yarkony, D. R. *J. Phys. Chem.* **1996**, *100*, 18612.
(20) German, K. R. *J. Chem. Phys.* **1976**, *64*, 4065.
(21) Lengel, R. K.; Crosley, D. R. *J. Chem. Phys.* **1978**, *68*, 5309.
(22) McDermid, I. S.; Laudenslager, J. B. *J. Chem. Phys.* **1982**, *76*, 1824.
(23) Copeland, R. A.; Dyer, M. J.; Crosley, D. R. *J. Chem. Phys.* **1985**, *82*, 4022.
(24) Copeland, R. A.; Wise, M. L.; Crosley, D. R. *J. Phys. Chem.* **1988**, *92*, 5710.
(25) Burris, J.; Butler, J.; McGee, T.; Heaps, W. *Chem. Phys.* **1991**, *151*, 233.

(26) Williams, L. R.; Crosley, D. R. *J. Chem. Phys*. **1996**, *104*, 6507.
(27) Fairchild, P. W.; Smith, G. P.; Crosley, D. R. *J. Chem. Phys*. **1983**, *79*, 1795.
(28) Smith, G. P.; Crosley, D. R. *J. Chem. Phys*. **1986**, *85*, 3896.
(29) Copeland, R. A.; Crosley, D. R. *J. Chem. Phys*. **1986**, *84*, 3099.
(30) Paul, P. H.; Durant, J. L.; Gray, J. A.; Furlanetto, M. R. *J. Chem. Phys*. **1995**, *102*, 8378.
(31) Paul, P. H. *J. Quant. Spectrosc. Radiat. Transfer* **1994**, *51*, 511.
(32) Burris, J.; Butler, J. J.; McGee, T. J.; Heaps, W. S. *Chem. Phys*. **1988**, *124*, 251.
(33) Paul, P. H. *J. Phys. Chem.* **1995**, *99*, 8472.
(34) Lester, M. I.; Loomis, R. A.; Giancarlo, L. C.; Berry, M. T.; Chakravarty, C.; Clary, D. C. *J. Chem. Phys*. **1993**, *98*, 9320.
(35) Offer, A. R.; van Hemert, M. C.; Vandishoeck, E. F. *J. Chem. Phys*. **1994**, *100*, 362.
(36) Schreel, K.; ter Meulen, J. J. *J. Chem. Phys*. **1996**, *105*, 4522.
(37) The results of Walch supercede the calculations of Miller et al., who predicted an excited-state well depth of 2300 cm^{-1}.[16]
(38) Hernández, R.; Clary, D. C. *Chem. Phys. Lett*. **1995**, *244*, 421.
(39) Loomis, R. A.; Lester, M. I. *Annu. Rev. Phys. Chem.* **1997**, *48*, 637.
(40) Leu, G.-H.; Hwang, C.-W.; Chen, I.-C. *Chem. Phys. Lett*. **1996**, *257*, 481.
(41) Walch, S. P.; Dunning, T. H. *J. Chem. Phys*. **1980**, *72*, 1303.
(42) Schatz, G. C.; Elgersma, H. *Chem. Phys. Lett*. **1980**, *73*, 21.
(43) The OH $P_1(1)$ line represents the transition energy between the lowest rotor levels in the ground X $^2\Pi_{3/2}$ ($v'' = 0$, $j'' = 1.5$) and excited A $^2\Sigma^+$ (v', $n' = 0$) states. Here, v'' and j'' denote the vibrational and total angular momentum quantum numbers for OH X $^2\Pi$, while v' and n' rotational angular momentum quantum numbers used to describe OH A $^2\Sigma^+$.
(44) German, K. R. *J. Chem. Phys*. **1975**, *63*, 5252.
(45) By analogy, *para*-D_2 ($j = 1$) is expected to be more strongly bound to OH X $^2\Pi$ than *ortho*-D_2 ($j = 0$). For D_2, however, the nuclear spin statistics favor *ortho* over *para* by a factor of 2:1. In this case, both *para*- and *ortho*-D_2−OH may contribute to the electronic excitation spectrum.
(46) Schwartz, R. L.; Anderson, D. T.; Todd, M. W.; Lester, M. I. *Chem. Phys. Lett*. **1997**, *273*, 18.
(47) Hernández, R. Personal communication.
(48) The rotor constants for *ortho*-H_2 and *para*-D_2 with OH X $^2\Pi$ were computed for the lowest intermolecular levels supported by the ground-state potential obtained in the MCKW ab initio calculation.[16] Recent infrared experiments have refined the value for the OH−H_2 ground-state rotational constant.[46]
(49) The OH−N_2 rotor constant was estimated by mass weighting the ground-state rotational constant of N_2−HF obtained from Lovejoy, C. M.; Nesbitt, D. J. *J. Chem. Phys*. **1987**, *86*, 3151.
(50) Kliesch, A. Ph.D. Thesis, Universität Bielefeld, 1994.
(51) Werner, H.-J.; Knowles, P. J. *J. Chem. Phys*. **1988**, *89*, 5803.
(52) Knowles, P. J.; Werner, H.-J. *Chem. Phys. Lett.* **1988**, *145*, 514.
(53) Dunning, Jr., T. H. *J. Chem. Phys.* **1989**, *90*, 1007.
(54) Talbi, D.; Saxon, R. P. *J. Chem. Phys.* **1989**, *91*, 2376.
(55) Shin, S. K.; Chen, Y.; Nickolaisen, S.; Sharpe, S. W.; Beaudet, R. A.; Wittig, C. *Adv. Photochem.* **1991**, *16*, 249.
(56) Bohmer, E.; Shin, S. K.; Chen, Y.; Wittig, C. *J. Chem. Phys*. **1992**, *97*, 2536.
(57) Kuppermann, A.; Wu, Y. S. M. *Chem. Phys. Lett*. **1993**, *205*, 577.
(58) Vegiri, A.; Farantos, S. C. *Mol. Phys.* **1990**, *69*, 129.
(59) Kudla, K.; Koures, A. G.; Harding, L. B.; Schatz, G. C. *J. Chem. Phys*. **1992**, 96, 7465.